Journal of Sound and Vibration (1999) **224**(1), 49–67
Article No. jsvi.1998.2113, available online at http://www.idealibrary.com on IDEAL®

SUPERSONIC FLUTTER ANALYSIS OF STIFFENED LAMINATED PLATES SUBJECT TO THERMAL LOAD

I. Lee, D.-M. Lee, and I.-K. Oh

Department of Aerospace Engineering, Korea Advanced Institute of Science and Technology, 373-1 *Kusong-dong*, *Yusong-gu*, *Taejon*, 305-701, *Korea*

(*Received* 29 *June* 1998, *and in final form* 24 *November* 1998)

Flutter analysis of stiffened laminated plates has been performed. The purpose of this study is to analyze the flutter characteristics of stiffened plates subject to thermal load. The first order shear deformable plate and Timoshenko beam theories are used for the finite element modelling of a skin panel and stiffeners respectively. The von Karman non-linear strain–displacement relation is used to account for large deflections. First order piston theory is used for modelling aerodynamic loads. The Newton–Raphson iteration method and complex eigenvalue solver with the LUM/NTF approximation method are used to obtain the postbuckled deflection and flutter information respectively. The Guyan reduction method and mode tracing procedure are employed for an efficient analysis. The effects of various parameters, such as the stiffening scheme, lamination angle, boundary conditions, and temperature gradient on flutter characteristics are investigated through some numerical examples. From these examples, it can be shown that the selection of a proper stiffening scheme results in great improvements of flutter characteristics of laminated panels without introducing considerable weight penalty.

1. INTRODUCTION

The stiffened panel is a useful and popular form of structural component in various engineering applications. Weight savings are an important consideration for high-performance structures. By using stiffened panels as primary structural components, light-weight and efficient structures can be obtained without considerable weight penalty. Also, structural components made of composite materials have a great potential for their utilization in a wide variety of efficient applications to meet the high-strength, high-stiffness, and minimum-weight requirement. Composite materials have been extensively used in stiffened structures of high-performance applications.

Also, thermal effect is important since temperature environment influences significantly the static and dynamic behaviors of flight structures in supersonic regime. Thermal buckling is induced by temperature increase due to

0022–460X/99/260049 + 19 $30.00/0

aerodynamic heating and restrained thermal expansion. It is well-known that thermal buckling does not mean ultimate failure of structures. The postbuckling load-carrying capacity of stiffened plates is generally very high. Such a postbuckling concept can be applied to advanced composite laminated structures in order to reduce structural weight. The results of many studies show that compressive loads induced by thermal effects could initiate flutter of a panel that would otherwise be stable. Therefore, the flutter analysis of stiffened composite laminated plates subject to thermal loads is necessary from the viewpoint of checking static and aeroelastic characteristics of structural components in supersonic regime. However, only a few investigations on panel flutter of stiffened laminated plates have dealt with thermal effects. Most of the published studies are concerned with flutter analysis of unstiffened panels with and without buckling loads.

An excellent presentation of fundamental theories and physical understanding of panel flutter can be found in two books [1, 2] and a review article [3] on the topic by Dowell. Linear and non-linear panel flutter analyses have been performed by Han and Yang [4], Hopkins and Dowell [5], Gray *et al*. [6], Xue and Mei [7], Zhou *et al*. [8, 9], Liaw [10], Liaw and Yang [11] and some other contributors [12–15]. In classical approaches of flutter analysis, Galerkin's method is used for the formulation of governing equations, and direct time-integration [1, 3], perturbation [13], and harmonic balance methods [14, 15] are used in the temporal domain analysis. However, these approaches take a relatively large amount of computation time or require lengthy and complex mathematical manipulations. The finite element method (FEM) is a powerful numerical tool for flutter analysis of isotropic and anisotropic panels with general geometry, applied loads, and boundary conditions. In several investigations, flutter analyses are performed through the use of the frequency domain (FD) approach such as the linearized updated mode/nonlinear time function (LUM/NTF) approximation method [6, 7] and direct time-integration (TI) method [8, 9]. The FD approach is efficient for parameter studies of panel flutter. However, it is very difficult to analyze the chaotic and nonperiodic motion accurately using the FD approach in the non linear flutter regime. In contrast, it is possible to analyze non periodic motions in a non linear flutter regime using the TI method. The TI method is useful for simulating the dynamic behavior of structures with a modern control system using adaptive materials such as piezolectric material [9]. However, the TI method is often too costly for finding flutter value and is inefficient for parameter study. Liao and Sun [16], and Lee and Lee [17] investigated the flutter characteristics of stiffened laminated panels. They discussed the effects of lamination scheme, stiffener size, and flow angle on flutter characteristics. However, in these studies, a thermal effect was not considered and a dynamic flutter deflection was assumed to be infinitesimal, that is, a linear flutter analysis without thermal effect was carried out.

In the present study, the flutter characteristics of stiffened laminated plates are analyzed with thermal effects. First order shear deformable plate theory (FSDT) and Timoshenko beam theory are used for the finite element

modelling of a skin panel and blade-type stiffeners respectively. For an efficient parametric study, the flutter analysis is performed using a frequency domain approach referred to as LUM/NTF. The von Karman non-linear strain–displacement relation is applied to account for a large deflection due to thermal loads. The first order piston theory is used for modeling aerodynamic loads. The Newton–Raphson iteration method is used to obtain statically deformed shape due to aerodynamic and thermal loads. The temperature change is assumed to be steady state. The degradation of material properties due to thermal effect is neglected.

2. MODELLING STIFFENED LAMINATED PLATE AND DERIVATION OF EQUATION OF MOTION

2.1. SKIN PLATE MODEL AND EQUATION OF MOTION

The strain–displacement relations in FSDT are given as

$$\{e\} = \{\varepsilon\} + z\{\kappa\} = \{\varepsilon_m\} + \{\varepsilon_\theta\} + z\{\kappa\}, \qquad \{\gamma\} = \{\gamma_{yz} \quad \gamma_{xz}\}^{\mathrm{T}}, \tag{1}$$

where

$$\{\varepsilon_m\} = \{u_{,x} \quad v_{,y} \quad u_{,y} + v_{,x}\}^{\mathrm{T}}, \qquad \{\varepsilon_\theta\} = \tfrac{1}{2}\{w_{,x}^2 \quad w_{,y}^2 \quad 2w_{,x}w_{,y}\}^{\mathrm{T}},$$

$$\{\kappa\} = \{\phi_{x,x} \quad \phi_{y,y} \quad \phi_{x,x} + \phi_{y,x}\}^{\mathrm{T}}, \qquad \{\gamma\} = \{w_{,y} + \phi_y \quad w_{,x} + \phi_x\}^{\mathrm{T}};$$

u, v, and w are the displacements in the x, y, and z directions respectively; ϕ_x and ϕ_y are rotation in the xz- and yz-planes respectively. The comma and subscript denote the partial derivative with respect to the subscript.

For an anisotropic plate subjected to any temperature change $\Delta T(x, y, z)$, the well-known constitutive relations can be obtained by integrating the stress–strain relation through the thickness of plates as:

$$\begin{Bmatrix} N \\ M \end{Bmatrix} = \begin{bmatrix} A & B \\ B & D \end{bmatrix} \begin{Bmatrix} \varepsilon \\ \kappa \end{Bmatrix} - \begin{Bmatrix} N_{\Delta T} \\ M_{\Delta T} \end{Bmatrix}, \quad \{Q\} = \begin{Bmatrix} Q_{yz} \\ Q_{xz} \end{Bmatrix} = \begin{bmatrix} A_{44} & A_{45} \\ A_{45} & A_{55} \end{bmatrix} \{\gamma\}, \tag{2}$$

where $\{N\}$ $\{M\}$, and $\{Q\}$ are in-plane load, moment, and transverse load vectors respectively; the thermal in-plane load and moment vectors are given as:

$$(\{N_{\Delta T}\}, \{M_{\Delta T}\}) = \sum_{k=1}^{n} \int_{k-1}^{z_k} [\overline{Q}]_k \{\bar{a}\}_k (1, z) \Delta T \, \mathrm{d}z.$$

The calculations of stiffness matrices $[A]$, $[B]$, $[D]$ and transverse shear stiffness A_{ij} can be easily found in the literature on laminated composite structures.

The element matrices and equations of motion are derived using the principle of virtual work:

$$\delta W = \delta W_{int} - \delta W_{ext} = 0 \tag{3}$$

The virtual work of the internal and external forces are given as:

$$\delta W_{int} = \int \{\delta e\}^{\mathrm{T}} \{\sigma\} \, \mathrm{d}V = \int_A (\{\delta\varepsilon\}^{\mathrm{T}} \{N\} + \{\delta\kappa\}^{\mathrm{T}} \{M\} + \{\delta\gamma\}^{\mathrm{T}} \{Q\}) \, \mathrm{d}A$$

$$= \{\delta \mathbf{d}\}^{\mathrm{T}}_{(e)} \left[[K] - [KT] + \tfrac{1}{2}[N1] + \tfrac{1}{3}[N2] \right]_{(e)} \{\mathbf{d}\}_{(e)} - \{\delta \mathbf{d}\}^{\mathrm{T}}_{(e)} \{P_{\Delta T}\}_{(e)},$$

$$\delta W_{ext} = \int_A [-I_0(\ddot{u}\delta u + \ddot{v}\delta v + \ddot{w}\delta w) - I_2(\ddot{\phi}_x \delta\phi_x + \ddot{\phi}_y \delta\phi_y) + p\delta w] \, \mathrm{d}A$$

$$= -\{\delta \mathbf{d}\}^{\mathrm{T}}_{(e)} [M]_{(e)} \{\ddot{\mathbf{d}}\}_{(e)} + \{\delta \mathbf{d}\}^{\mathrm{T}}_{(e)} \{f\}_{(e)}, \tag{4}$$

where δ denotes variation; (e) represents elementary form; $\{\mathbf{d}\}_{(e)}$ is the displacement vector of the element, $\{\mathbf{d}\}_{(e)} = \{u, v, w, \phi_x, \phi_y\}^{\mathrm{T}}$; $[K]$ and $[KT]$ are linear elastic stiffness and linear thermal stiffness respectively; $[N1]$ and $[N2]$ are the first and second order non-linear stiffness due to large deflection, $\{f\}$ and $\{P_{\Delta T}\}$ are external force and thermal load vector, mass properties are defined as follows:

$$(I_0, I_2) = \int_{-c/2}^{c/2} \rho(1, z^2) \, \mathrm{d}z$$

where c and ρ are the thickness and material density of a panel. The detailed derivation and expression of the matrices in equation (4) can be found in reference 18.

By substituting equation (4) into (3) and assembling the element matrix and vectors, the equation of motion for a plate can be obtained in global coordinates:

$$[M]\{\ddot{\mathbf{d}}\} + [[K] - [KT] + \tfrac{1}{2}[N1] + \tfrac{1}{3}[N2]]\{\mathbf{d}\} = \{f\} + \{P_{\Delta T}\}. \tag{5}$$

2.2. STIFFENER MODEL

Anisotropic stiffeners along the x-axis are modelled using Timoshenko beam elements to maintain the compatibility between the skin plate and stiffeners (see Figure 1). The displacement field of the stiffeners is assumed to be

$$u_b = u_0 - e\phi_x + z\phi_x, \qquad v_b = v_0 + z\phi_y, \qquad w_b = w_0 - y\phi_y \tag{6}$$

where e is the eccentricity of the stiffener and the subscript 0 denotes the midplane value of the skin plate. The strain–displacement relations can be given as:

$$\{e^b\} = \{e_m\} + \{e_n\} + \{e_r\}, \qquad \gamma^b_{xy} = \nu_{0,x} + z\phi_{y,x}, \tag{7}$$

where

$$\{e_m\} = \{u_{0,x} - e\phi_{x,x} \quad \phi_x + w_{0,x}\}^{\mathrm{T}}, \qquad \{e_n\} = \tfrac{1}{2}\{(w_{0,x})^2 \; 0\},$$

$$\{e_r\} = \{z\phi_{x,x} \quad -y\phi_{y,x}\}^{\mathrm{T}},$$

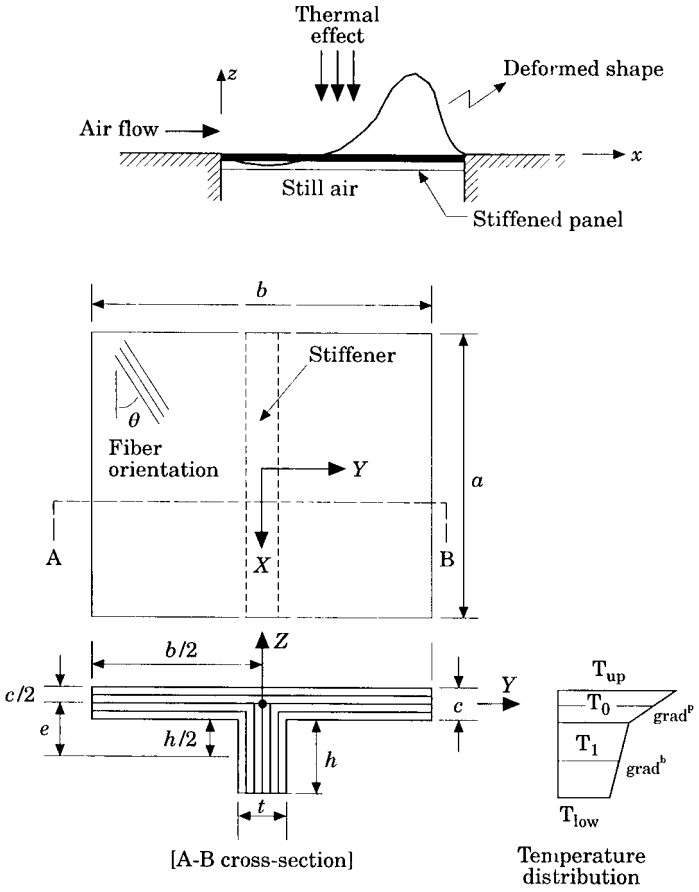

Figure 1. Schematic diagram of stiffened panel subject to aero–thermal load.

and ,x denotes the partial derivative with respect to x, and the superscript b means stiffener. When the widths and heights of stiffeners are much smaller than their lengths, one assumes $\sigma_y \approx 0$ and $\sigma_z \approx 0$ in the stiffeners. Taking the coordinates of the laminated stiffener into account (Figure 1), the constitutive equations for a stiffener are:

$$\begin{Bmatrix} \sigma_x^b \\ \tau_{xz}^b \end{Bmatrix} = \begin{bmatrix} C_{11} & C_{16} \\ C_{16} & C_{66} \end{bmatrix} \left(\begin{Bmatrix} e_x^b \\ \gamma_{xz}^b \end{Bmatrix} - \begin{Bmatrix} \alpha_x^b \\ \alpha_{xz}^b \end{Bmatrix} \Delta T \right), \qquad \tau_{xy}^b = C_{55}\gamma_{xy}^b, \tag{8}$$

where the stiffness coefficients C_{ij} are called modified reduced stiffnesses and the relation between the stiffness coefficients can be found in reference [19].

To derive the stiffness, mass matrices and thermal load vector for stiffeners, one can use the variational form of strain energy δU and kinetic energy δK as:

$$\delta U = \int_x \int_A (\delta\{e^b\}^{\mathrm{T}}[C]\{e^b\} + \delta\gamma_{xy}^b C_{55}\gamma_{xy}^b - \delta\{e^b\}^{\mathrm{T}}[C]\{\alpha^b\}\Delta T)\, \mathrm{d}A\, \mathrm{d}x,$$

$$\delta K = \int_x \int_A (\dot{u}_b\delta\dot{u}_b + \dot{v}_b\delta\dot{v}_b + \dot{w}_b\delta\dot{w}_b)\, \mathrm{d}A\, \mathrm{d}x. \tag{9}$$

The derivation of linear stiffness and mass matrices can be found in reference [19] and the derivation procedure of non-linear stiffness is similar to that of linear stiffness. Using the same shape functions as the plate element, the element matrices and vector of a stiffener can be obtained from equation (9). The whole matrices and vector for a stiffened plate are given as:

$$[K_{tot}] = [K^p_{tot}] + [K^b_{tot}], \quad [M] = [M^p] + [M^b], \quad \{P_{\Delta T}\} = \{P^p_{\Delta T}\} + \{P^b_{\Delta T}\} \tag{10}$$

where $[K_{tot}]$ is total stiffness including linear and non-linear terms, and superscripts p and b denote skin plate and stiffener respectively. Substituting equation (10) into (5), one can obtain the equation of motion for a stiffened laminated plate which is of identical form to equation (5) as:

$$[M]\{\ddot{\mathbf{d}}\} + [[K] - [KT] + \tfrac{1}{2}[N1] + \tfrac{1}{3}[N2]]\{\mathbf{d}\} = \{f\} + \{P_{\Delta T}\}. \tag{11}$$

2.3. AERODYNAMIC LOAD MODEL

The aerodynamic force and damping matrices can be derived using virtual work done by the aerodynamic load p as:

$$\int_A p\delta w \, \mathrm{d}A = \int_A \left(-\beta \frac{\partial w}{\partial x} - g\frac{\partial w}{\partial t}\right)\delta w \, \mathrm{d}A \tag{12}$$

where β and g are the aerodynamic pressure parameter and damping parameter; w is the transverse deflection of skin panel. β and g are referred to in reference 4. Applying a F.E.M. shape function to equation (12), one obtains the nodal force vector with respect to the transverse deflection, w as:

$$\{f\} = -\beta[A_f]\{w\} - g[A_d]\{\dot{w}\}. \tag{13}$$

By substituting equation (13) into equation (11), one obtains the following equation of motion for a stiffened panel subject to aerodynamic and thermal loads:

$$[M]\{\ddot{\mathbf{d}}\} + g[AD]\{\dot{\mathbf{d}}\} + [[K] - [KT] + \beta[AF] + \tfrac{1}{2}[N1] + \tfrac{1}{3}[N2]]\{\mathbf{d}\} = \{P_{\Delta T}\} \tag{14}$$

where

$$[AF] = \begin{bmatrix} [0]_m & [0] & [0] \\ [0] & [A_f]_b & [0] \\ [0] & [0] & [0]_p \end{bmatrix}, \quad [AD] = \begin{bmatrix} [0]_m & [0] & [0] \\ [0] & [A_d]_b & [0] \\ [0] & [0] & [0]_p \end{bmatrix}$$

where subscripts m, b, and p denote values with respect to in-plane, transverse, and rotational displacements respectively. In Equation (14), $[AF]$ and $[AD]$ are named as aerodynamic force and damping matrices.

3. SCHEME FOR POSTBUCKLING AND FLUTTER ANALYSIS

To analyze the flutter of buckled plates due to thermal load, the solution of a governing equation (14) is assumed to be the sum of a time-dependent solution

and a time-independent solution such as $\{\mathbf{d}\} = \{\mathbf{d}_t\} + \{\mathbf{d}_s\}$, where $\{\mathbf{d}_t\}$ is the time-dependent solution and $\{\mathbf{d}_s\}$ is the statically trimmed solution. Substituting this assumed solution into the equation of motion, two coupled equations can be obtained as [18]:

$$[[K] - [KT] + \beta[AF] + \tfrac{1}{2}[N1]_s + \tfrac{1}{3}[N2]_s]\{\mathbf{d}_s\} = \{P_{\Delta T}\}, \tag{15}$$

$$\begin{aligned}[M]\{\ddot{\mathbf{d}}_t\} + g[AD]\{\dot{\mathbf{d}}_t\} + [[K] = [KT] + \beta[AF] + [N1]_s + [N2]_s \\ + [N2]_{st} + \tfrac{1}{2}[N1]_t + \tfrac{1}{3}[N2]_t]\{\mathbf{d}_t\} = \{0\}\end{aligned} \tag{16}$$

where subscripts s and t denote static and dynamic values, respectively.

3.1. REDUCED GOVERNING EQUATION OF POSTBUCKLING BEHAVIOR

Using the Newton–Raphson iteration method, the incremental form of the non-linear equation can be derived from equation (15) as:

$$[[K] - [KT] + \beta[AF] + [N1]_s + [N2]_s]_i\{\Delta\mathbf{d}_s\}_{i+1} = \{\Delta f\}_i, \tag{17}$$

where the incremental force vector and updated displacement vector are:

$$\{\Delta f\}_f = \{P_{\Delta T}\} - [[K] - [KT] + \beta[AF] + \tfrac{1}{2}[N1]_s + \tfrac{1}{3}[N2]_s]\{\mathbf{d}_s\}_i,$$

$$\{\mathbf{d}_s\}_{i+1} = \{\mathbf{d}_s\}_i + \{\Delta\mathbf{d}_s\}_{i+1}.$$

For efficiency of numerical analysis, equation (17) is reduced by applying static condensation to:

$$[RK0]\{\Delta w_s\}_{i+1} = \{\Delta R\}_i, \tag{18}$$

where

$$\begin{aligned}[RKO] = [K_b] - [K_{\Delta T}] + \beta[A_f] + [N1_b]_s + [N2_b]_s \\ - \begin{bmatrix}[N1_{mb}] \\ [K_{pb} + N1_{pb}]\end{bmatrix}^{\mathrm{T}} \begin{bmatrix}[K_m] & [K_{mp}] \\ [K_{pm}] & [K_p]\end{bmatrix}^{-1} \begin{bmatrix}[N1_{mb}] \\ [K_{pb} + N1_{pb}]\end{bmatrix}\end{aligned}$$

and $[K_{\Delta T}]$ is the reduced thermal stiffness matrix for $[KT]$. The reduced vector of incremental force and updated transverse displacement are:

$$\{\Delta R\}_i = \left\{\{\Delta f_b\} - \begin{bmatrix}[N1_{mb}] \\ [K_{pb} + N1_{pb}]\end{bmatrix}^{\mathrm{T}} \begin{bmatrix}[K_m] & [K_{mp}] \\ [K_{pm}] & [K_p]\end{bmatrix}^{-1} \begin{Bmatrix}\{\Delta f_m\} \\ \{\Delta f_p\}\end{Bmatrix}\right\},$$

$$\{w_s\}_{i+1} = \{w_s\}_i + \{\Delta w_s\}_{i+1}.$$

For recovery of deleted DOFs, the following equation is used:

$$\begin{Bmatrix} \{\Delta u\} \\ \{\Delta \phi\} \end{Bmatrix}_i = -\begin{bmatrix} [K_m] & [K_{mp}] \\ [K_{pm} & [K_p] \end{bmatrix}^{-1} \begin{bmatrix} [N1_{mb}] \\ [K_{pb} + N1_{pb}] \end{bmatrix} \{\Delta w\}_i + \begin{bmatrix} [K_m] & [K_{mp} \\ [K_{pm} & [K_p] \end{bmatrix}^{-1} \begin{Bmatrix} \{\Delta f_m\} \\ \{\Delta f_p\} \end{Bmatrix}_i, \tag{19}$$

where $\{u\}$, $\{w\}$, and $\{\phi\}$ are in-plane, transverse, and rotational displacements respectively.

3.2. REDUCED FLUTTER EQUATION

For numerical efficiency of flutter analysis, equation (16) is reduced by applying the Guyan reduction method with respect to in-plane and rotation DOFs as shown in the previous section to:

$$[RM]\{\ddot{w}_t\} + g[A_d]\{\dot{w}_t\} + [\,[RK0] + [RK1] + [RK2]\,]_t\{w_t\} = \{0\}, \tag{20}$$

where the details of reduced matrices and recovery DOFs are given in the Appendix. In the above, [*RK0*], [*RK1*], and [*RK2*] are constant stiffness, first order, and second order non-linear stiffness matrices dependent on displacements. An iterative method in the frequency domain based on LUM/NTF approximation by Xue and Mei [7] is applied in this study. In this approximation, dynamic displacements are assumed to be harmonic oscillation as follows:

$$\{w_t\} = \lambda\{\bar{w}\}\cos\omega t \tag{21}$$

where $\{\bar{w}\}$ is a normalized complex vector whose maximum value is unity. λ represents the maximum amplitude of transverse deflection. By substituting equation (21) into equation (20) and applying LUM/NTF to equation (20), the following equation for flutter analysis can be obtained:

$$([RK0] + (\lambda/\sqrt{2})[\overline{RK1}] + 3\lambda^2/4[\overline{RK2}] + \omega^2[RM])\{\bar{w}\} = \{0\}, \tag{22}$$

where $[\bar{}\,]$ denotes stiffness matrix dependent on an eigenvector $\{\bar{w}\}$ and the aerodynamic damping term is assumed to be negligible. The details of the LUM/NTF can be found in references [6] and [7]. Linear flutter equation is obtained by eliminating the non-linear terms in equation (22).

For simple presentation of analysis results, the following non-dimensional parameters are introduced [4].

$$\beta^* = \beta a^3/D, \qquad \omega^* = \omega_i\sqrt{a^4\rho c/D} \tag{23}$$

where β^* and ω^* are non-dimensional dynamic pressure and frequency, a and c are side length and thickness of skin panel; D is rigidity of panel ($D = Ec^3/12(1-\nu^2)$ for isotropic material and $D = E_2c^3$ for anisotropic material).

3.3. MODE TRACING SCHEME

For clear and precise computation of linear and non-linear flutter problems, a mode tracing scheme is used at every step in the increment of dynamic pressure β. By using this scheme, the correlation of modes between previous and present steps can be found. The tracing scheme is performed using scalar product of eigenvectors between previous and present steps as:

$$\{\bar{w}_{k-1}^{(i)}\}^{\mathrm{T}} \cdot \{\bar{w}_{k}^{(i)}\} = T_{ij}, \tag{24}$$

where $\{\bar{w}_{k-1}^{(i)}\}$ represents the ith eigenvector at the calculation step $k-1$. When the value of T_{ij} is maximised or is near unity, the ith eigenvector in the previous step is correlated with the jth in the present step. The change of frequencies versus aerodynamic pressure is very complicated without a mode tracing scheme as shown in Figure 2(a). By using a mode tracing scheme, mode histories are clear and the coalescence of flutter modes is distinct as shown in Figure 2(b). Additionally, precise application of mode to non-linear stiffness is important because non-linear stiffness is a function of a specific mode. By using the tracing scheme, the precise application of mode can be achieved. Moreover, flutter analysis with a mode tracing scheme is very efficient because flutter calculation related to only the flutter mode can be performed in the limit-cycle flutter problem.

3.4. TEMPERATURE DISTRIBUTION

The distribution of temperature change is assumed to be uniform in the x–y plane and linear in the z direction as follows (Figure 1):

$$\Delta T^{p} = \Delta T_0(1 + \mathrm{grad}^{p}(z/c)), \quad \Delta T^{b} = \Delta T_1(1 + \mathrm{grad}^{b}((z+e)/h)), \tag{25}$$

where grad is temperature gradient in the z direction; ΔT_0 and ΔT_1 are mean temperature changes; superscripts p and b denote skin panel and stiffener and e and h are eccentricity and height of stiffener. Temperatures at the junction between the skin plate and stiffeners are identical. Temperature values in this study are non-dimensionalized as $\Delta T^{*} = \Delta T_0/\Delta T_{cr}$. Here, ΔT_{cr} is determined

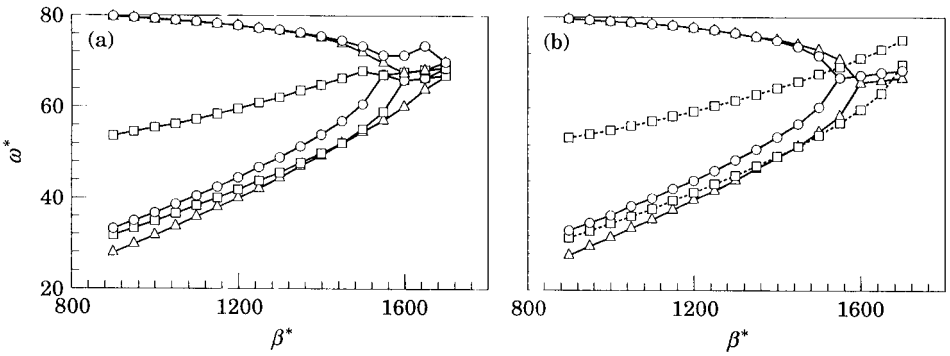

Figure 2. Mode tracing process in flutter analysis of stiffened plate ($\Delta T^{*} = 1{\cdot}25$, $a/b = 1$, ?$a/c = 150$, $t/c = 1$, $h/c = 3$, $[0_2/90_2]_s$): (a) without mode tracing; (b) with mode tracing.

from the thermal Euler buckling analysis of a stiffened composite plate in the state of unit uniform (0 gradient) temperature distribution.

4. RESULTS AND DISCUSSION

Material properties of graphite-epoxy laminar in this study are: $E_1 = 155{\cdot}0$ Gpa, $E_2 = 8{\cdot}07$ Gpa, $G_{12} = G_{13} = 4{\cdot}55$ Gpa, $G_{23} = 3{\cdot}25$ Gpa, $\nu_{12} = 0{\cdot}22$, $\alpha_1(\times 10^{-6}\ \text{m/m/°C}) = -0{\cdot}07$, $\alpha_2(\times 10^{-6}\ \text{m/m/°C}) = 30{\cdot}1$.

The dimensions and temperature gradients of a typical stiffened plate are given as: $a/b = 1{\cdot}5$, $a/c = 300$, $t/c = 1{\cdot}0$, $h/c = 3{\cdot}0$; lamination scheme = $[0_2/90_2]_s$ for skin panel and stiffeners; grad = 10% and 2% for skin panel and stiffeners, respectively; the boundary condition (simply supported in all edges) is

$$\text{S.S. on x-axis: } u = v = w = \phi_x = 0 \text{ and } \phi_y \neq 0;$$

$$\text{S.S. on y-axis: } u = v = w = \phi_y = 0 \text{ and } \phi_x \neq 0. \tag{26}$$

In the above, t and h are thickness and height of a stiffener respectively. Every stiffener is attached to the skin panel with equivalent spacing. The airflow direction is assumed to be parallel to stiffeners.

4.1. VERIFICATION OF ANALYSIS CODE

The well-known numerical integration results by Dowell [1–3] and FD results by Xue and Mei [7] are used as a reference to prove the accuracy of the present finite element code for flutter analysis. The isotropic plate ($\nu = 0{\cdot}3$) is subject to uniform temperature in all directions and boundary conditions are simply supported. The finite element solutions by Xue and Mei are obtained using the 24-DOF rectangular element based on classical plate theory (3×8 half-plate mesh). The present finite element solutions are obtained using 5×5 nine-noded

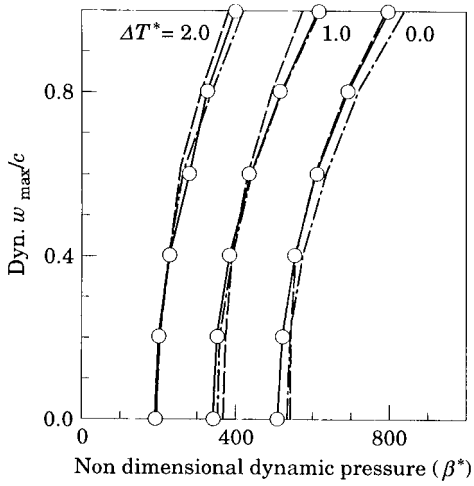

Figure 3. Limit-cycle amplitude versus dynamic pressure in isotropic square plate with simply-supported boundary conditions ($\nu = 0{\cdot}3$). Key: —○—, present; – – –, Dowell (time integration using six modes; — - —, Xue and Mei (6×8 ftm).

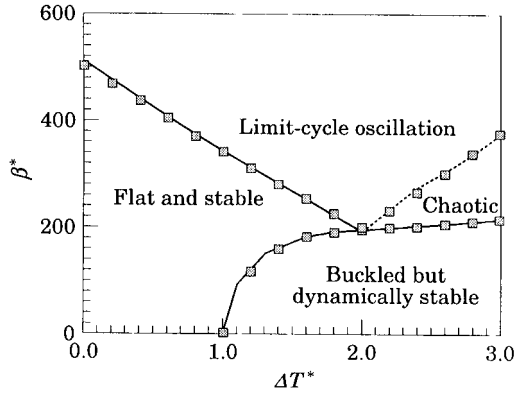

Figure 4. Stability boundaries of isotropic square plate. Key: —, present; ■, Xue and Mei.

quadrilateral elements based on FSDT (full-plate mesh). Figures 3 and 4 show good agreements between the results referred to and the present ones for limit-cycle flutter values and stability boundaries of the isotropic plate.

4.2. AERO–THERMAL POSTBUCKLING BEHAVIOR

Figure 5 shows maximum static deflections of stiffened and unstiffened laminated plates with and without temperature gradient. The bifurcation buckling does not occur under the existence of temperature gradient or eccentrically attached stiffeners. In the stiffened panel, the static deflection at flutter onset point does not become zero due to bending moment induced by eccentricity of stiffener at any temperature gradient. Flutter points are obtained from the linear flutter analysis. Figure 6 shows the postbuckling deflection of a stiffened plate with three stiffeners at various dynamic pressures and at $\Delta T^* = 2{\cdot}0$. The maximum deflection occurs at 75% of the length of the skin panel near flutter point ($\beta^* = 1000$). The increase of thermal load causes the maximum buckled deflections to become larger and the increase of dynamic pressure reduces the deflections as shown in Figure 7.

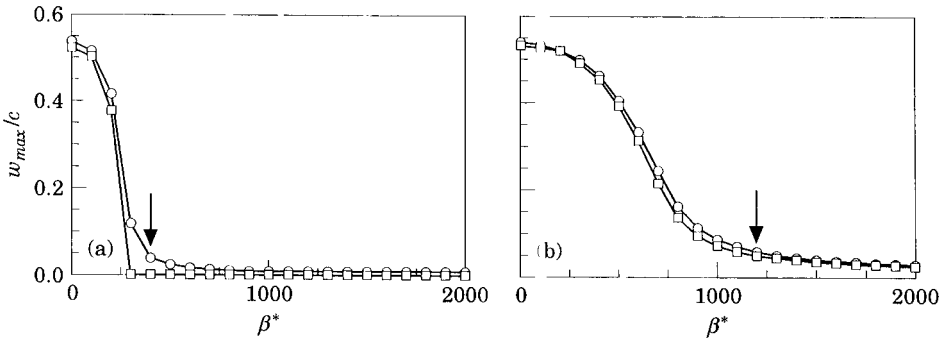

Figure 5. Maximum static deflections of laminated panels subject to aero-thermal load ($\Delta T^* = 2{\cdot}0$). (a) unstiffened panel; (b) stiffened panel. Key: —○—, grad = 10%; —■—, grad = 0%.

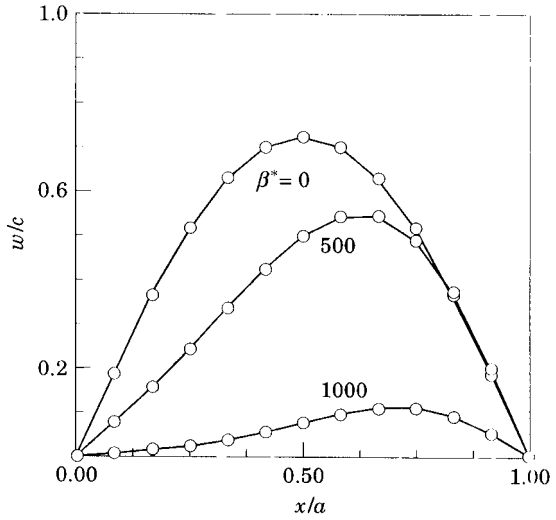

Figure 6. Static deflections of stiffened laminated panel (lamination $0_2/90_2)_s$ at $y/b = 0{\cdot}5$, $\Delta T^* = 2{\cdot}0$, $a/b = 1{\cdot}5$, $a/c = 300$, $t/c = 1$, $h/c = 3$.

4.3. MODE COALESCENCE IN STIFFENED PANEL

It is well-known that the first and the second mode, or the first and the third mode coalesce first in an unstiffened laminated panel. However, in a stiffened panel, the first coalescence of natural frequencies may occur in the higher modes than the above-mentioned modes as shown in Figure 8. The dimensions of stiffened plates are given in Equation (26). The attached stiffeners result in significant changes of natural frequencies of panel according to the increase of dynamic pressure as shown in Figure 8.

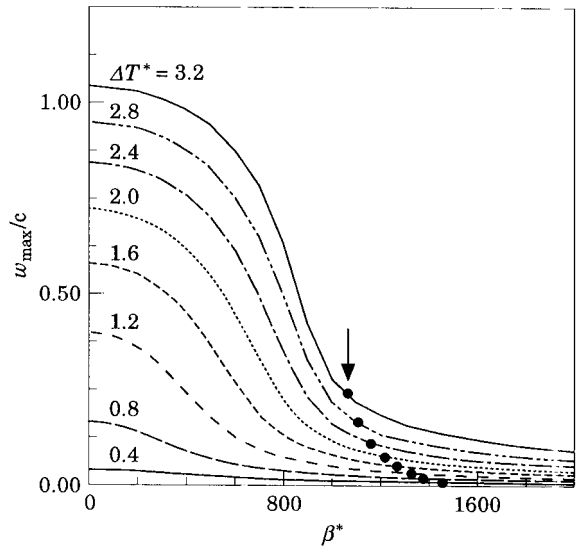

Figure 7. Maximum static deflections of panel $(0_2/90_2)_s$ with three stiffeners subject to aerothermal load: $a/b = 1{\cdot}5$, $a/c = 300$, $t/c = 1$, $h/c = 3$.

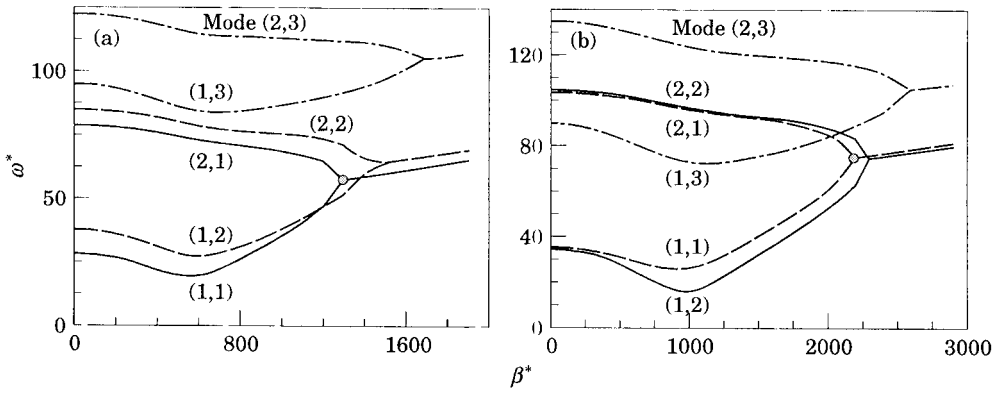

Figure 8. Mode coalescence in flutter analysis of stiffened plates when $\Delta T^* = 1{\cdot}5$: lamination and dimensions as for Figure 6. (a) Three stiffeners; (b) seven stiffeners.

4.4. EFFECT OF ATTACHED STIFFENERS ON FLUTTER BOUNDARY

Two kinds of stiffened plates are considered as examples: stiffened plates with three stiffeners (added mass = 4·5% of skin panel mass) and seven stiffeners (added mass = 10·5% of skin panel mass). The dimensions of the stiffened plates are given in equation (26). The dimensions of the unstiffened plate are equal to those of the skin panel of stiffened plates. Also, the unstiffened plate with equivalent mass to the stiffened plate with seven stiffeners (EUP) is considered. Figure 9 shows the flutter boundaries of these four kinds of panels. Every non-dimensional value is calculated using the values of the unstiffened plate. Compared with the flutter boundary of the EUP, that of the stiffened plates rises conspicuously. The increase in the number of stiffeners results in the direct increase of flutter onset points as shown in Figure 9.

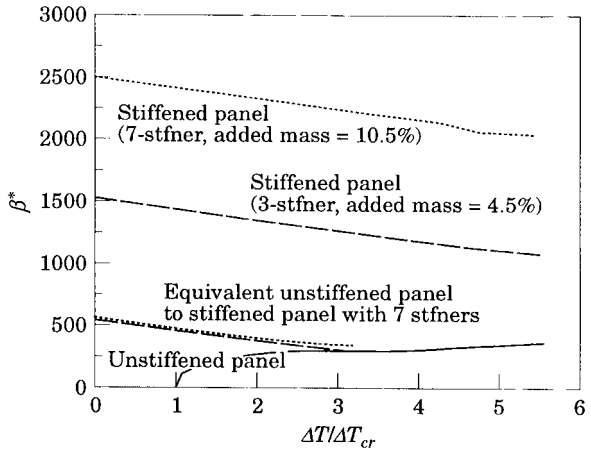

Figure 9. Comparison of flutter boundaries between unstiffened and stiffened graphite–epoxy $(0_2/90_2)_s$ plates ($a/b = 1{\cdot}5$, $a/c = 300$, $t/c = 1$, $h/c = 3$), ΔT_{cr} is value of unstiffened plate.

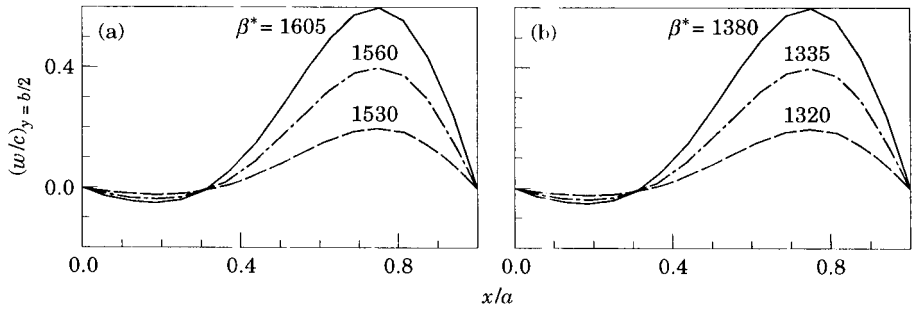

Figure 10. Aerodynamic load and flutter amplitude/frequency for stiffened plate $(0_2/90_2)_s$. (a) $\Delta T^* = 0{\cdot}0$, no static deflection: key for ω^* values; – – –, 68·07; — - —, 69·19; ————, 70·90. (b) $\Delta T^* = 2{\cdot}0$: key; – – –, $\omega^* = 58{\cdot}80$, $(w_{max}/c)_{stat} = 0{\cdot}0329$; — - —, $\omega^* = 60{\cdot}28$, $(w_{max}/c)_{stat} = 0{\cdot}0324$; ————, $\omega^* = 62{\cdot}55$, $(w_{max}/c)_{stat} = 0{\cdot}311$.

4.5. LIMIT-CYCLE DEFLECTION VERSUS DYNAMIC PRESSURE

Figure 10 shows the typical limit-cycle deflection shapes of the stiffened panel with three stiffeners. The stiffened plate is subject to thermal load at $\Delta T^* = 1{\cdot}2$ and various dynamic pressures. The maximum deflections occur at 75% of the panel length. Under the existence of thermal load, the postbuckled static deflection of the stiffened plate does not completely vanish in the limit-cycle flutter range. As the dynamic pressure increases, the corresponding limit-cycle amplitudes and frequencies become higher as shown in Figure 10.

4.6. EFFECT OF TEMPERATURE GRADIENT

The dimensions of the stiffened plate are equal to those of Equation (26). The value of grad in stiffeners is constantly 2%, but those in the skin panel are 0%, 10%, 30%, and 50%. Table 1 shows the flutter onset values, the corresponding maximum static deflections, and flutter frequencies for the stiffened plate with three stiffeners for various temperature gradients in the skin panel. Though the temperature gradient becomes higher, there are little changes in the flutter onset values and corresponding frequencies. Accordingly, the effect of temperature gradient on flutter boundary is insignificant as shown in Table 1.

TABLE 1

Effect of temperature gradient on flutter values of stiffened plate

ΔT^*	grad_{sk} (%)	$(w/c)^a$	ω^*_{cr}	β^*_{cr}	merging mode
0·5	0	0·0093	64·95	1402·6	
	10	0·0107	64·96	1402·8	
	30	0·0142	64·98	1403·3	
	50	0·0184	64·99	1403·8	1 and 3
1·5	0	0·0394	56·54	1251·3	modes
	10	0·0452	56·60	1252·4	
	30	0·0613	56·74	1254·8	
	50	0·0810	56·92	1257·4	

$(\,)^a$ denotes static deflection in flutter onset point.

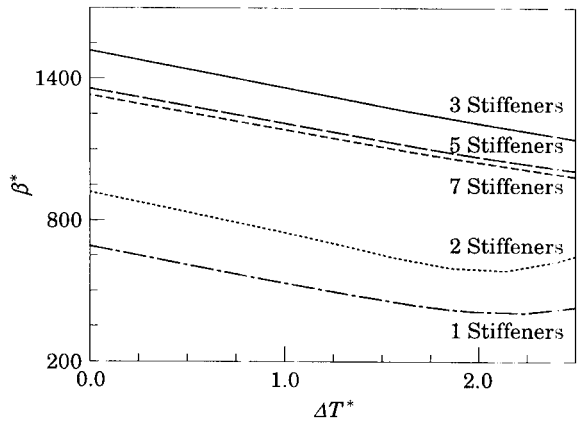

Figure 11. Effect of stiffening scheme on flutter dynamic pressure of stiffened plates ($a/b = 1{\cdot}5$, $a/c = 150$, lamination = $[0_2/90_2]_s$, simply-supported). Key: ——, $t/c = 1$, $h/c = 3$; – – –, $t/c = 0{\cdot}6$, $h/c = 3$; - - - -, $t/c = 0{\cdot}43$, $h/c = 3$; ·····, $t/c = 1{\cdot}125$, $h/c = 4$; — · —, $t/c = 1{\cdot}8$, $h/c = 5$.

4.7. EFFECT OF STIFFENING SCHEME

Total added mass due to attached stiffeners is constant in any stiffened plate in this section. Added mass is 4·5% of the mass of the skin panel. The dimensions of the skin panel are like those of equation (26). Those of the stiffeners are given in the inset of Figure 11. Figure 12 shows the flutter mode shapes of various stiffened laminated plates. The stiffener in stiffened plates with single stiffener and double stiffeners functions nearly as a rigid boundary as shown in Figure 12. However, the flutter boundaries of stiffened plates with three or more stiffeners are higher than those of stiffened plates with a single or

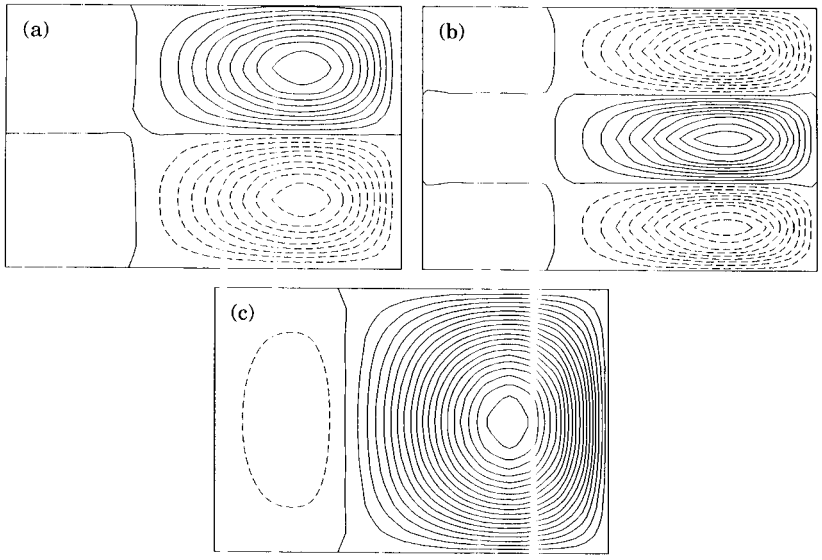

Figure 12. Flutter mode shape of various stiffened plates. (a) Single stiffeners; (b) double stiffener; (c) three or more stiffeners.

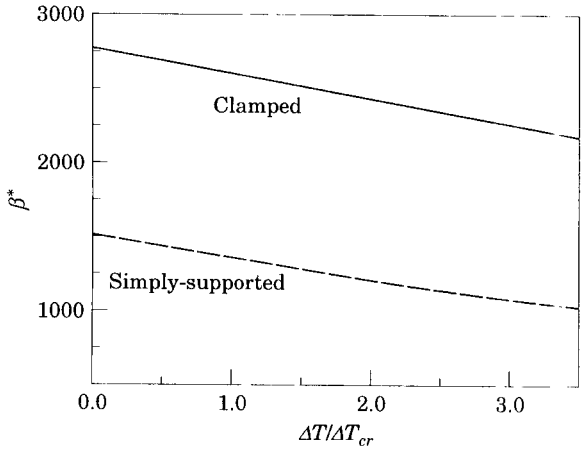

Figure 13. Flutter boundaries of stiffened plates ($(0_2/90_2)_s$ with three stiffeners) with simply-supported and clamped. Added mass = 4·5% of skin panel mass; $a/b = 1{\cdot}5$; $a/c = 300$; $t/c = 1$; $h/c = 3$.

double stiffeners. Figure 11 shows that the stiffened plate with three stiffeners produces the best flutter characteristics. The stiffening scheme directly influences the flutter characteristics as shown in Figure 11. Therefore, the proper stiffening scheme should be selected to obtain the optimum flutter boundary.

4.8. EFFECT OF BOUNDARY CONDITION

The dimensions of the stiffened panel in this example are the same as those of equation (26). Non-dimensional temperature is calculated using the critical temperature of the simply supported panel. Figure 13 shows the flutter boundary for two different boundary conditions: simply supported and clamped at all edges. The stiffened plate with more restrained boundary condition is more stable as expected. The clamped panel has a much higher flutter boundary than the simply supported panel as shown in Figure 13.

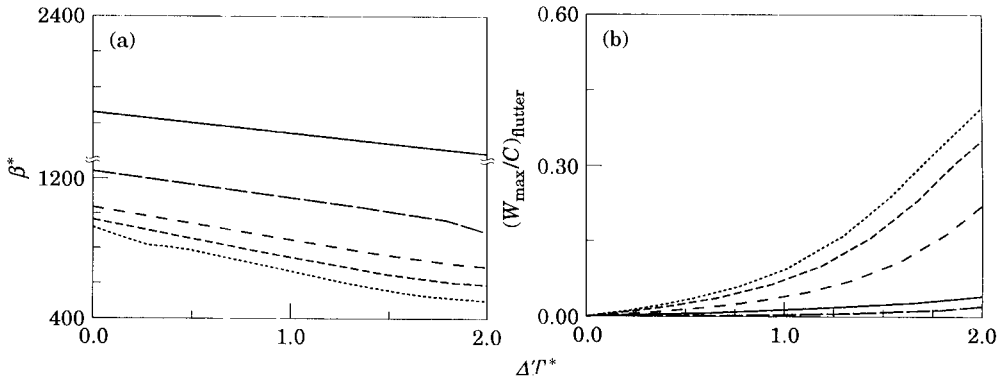

Figure 14. Effect of fiber orientation on flutter boundary and static deflections at flutter onset point for stiffened plates with 3 stiffeners and simply-supported ($a/b = 1{\cdot}5$, $a/c = 150$, $t/c = 1$, $h/c = 3$, lamination = $(0/90/\pm\theta)_s$). (a) Flutter boundaries; (b) maximum static deflections. Key for orientation $\theta°$: ——, 0; — —, 30; – – –, 45; - - - -, 60; ·····, 90.

4.9. EFFECT OF LAMINATION SCHEME

The effect of fiber orientation θ on flutter values is investigated in this example. The range of fiber orientation is taken between 0° and 90°. The dimensions of stiffened plates are also equal to those of equation (26). The lamination scheme of the skin panel and stiffeners of the plates is $[0/90/\pm\theta]_s$. The non-dimensional thermal load is calculated using the values of case $\theta = 0$. Figure 14 shows the flutter boundaries and maximum static deflections at flutter onset points at various temperatures and dynamic pressures. As the fiber orientation angle changes from 0° to 90°, the stable region reduces monotonically and static deflection at the flutter onset point increases due to lower critical dynamic pressure as shown in Figure 14. Flutter mode shapes of these various stiffened plates are similar to those of $[0_2/90_2]_s$ stiffened plate with three stiffeners in Figure 12.

5. CONCLUSION

A supersonic flutter analysis of stiffened laminated plates has been performed using the finite element method, developed on the basis of first order shear deformable theory, Timoshenko beam theory, the von Karman strain–displacement relation, and first order piston theory. Numerical results were obtained using the Newton–Raphson iteration method for an aero–thermal postbuckling analysis and complex eigenvalue solution procedure with application of LUM/NTF for a flutter analysis. The Guyan reduction method is employed to reduce the problem size and computational time. Using the mode tracing procedure, an efficient and precise computation in linear and non-linear flutter analysis can be carried out. Limit-cycle flutter results and stability boundaries for unstiffened isotropic plates were compared with those published and good agreement between them was found.

The present investigations were mainly focused on the effect of attached stiffeners on flutter characteristics. The present results illustrated quantitatively the effects of number of stiffeners, stiffening scheme, fiber orientation, boundary conditions, and temperature gradient on flutter boundary. From these results, it can be easily found that the flutter characteristics of panels can be improved remarkably by using the proper stiffening scheme without increase in mass. The flutter characteristics of stiffened panels are sensitive to the stiffening scheme, magnitude of thermal load, fiber orientation, and boundary conditions. However, temperature gradient has a minor effect on flutter bounds of stiffened panels.

REFERENCES

1. E. H. DOWELL 1975 *Aeroelasticity of Plates and Shell*. Leyden: Noordhoff International Publishing.
2. E. H. DOWELL and M. ILGAMOV 1988 *Studies in Nonlinear Aeroelasticity*. Berlin: Springer-Verlag.

3. E. H. DOWELL 1970 *AIAA Journal* **8**, 385–399. Panel flutter: a review of the aeroelastic stability of plates and shells.
4. A. D HAN and T. Y. YANG 1983 *AIAA Journal* **21**, 1453–1461 Nonlinear panel flutter using high order triangular finite elements.
5. M. A. HOPKINS and E. H. DOWELL 1994 *Proceedings of the AIAA/ASME/ASCE/AHS/ASC 35th SDM Conference*, AIAA-94-1486, 1343–1355. Limited amplitude panel flutter with a temperature differential.
6. C. E. GRAY Jr., C. MEI and C. P. SHORE 1991 *AIAA Journal* **29**, 290–298. Finite element method for large amplitude two-dimensional panel flutter at hypersonic speeds.
7. D. Y. XUE and C. MEI 1993 *AIAA Journal* **31**, 154–162 Finite element nonlinear panel flutter with arbitrary temperatures in supersonic flow.
8. R. C. ZHOU, D. Y. XUE and C. MEI 1994 *AIAA Journal* **32**, 2044–2052. Finite element time domain-modal formulation for nonlinear flutter of composite panels.
9. R. C. ZHOU 1995 *AIAA Journal* **33**, 1098–1105. Suppression of nonlinear panel flutter with piezoelectric actuators using finite element method.
10. D. G. LIAW 1993 *AIAA Journal* **30**, 105–111. Supersonic flutter of laminated thin plates with thermal effects.
11. D. G. LIAW and H. T. Y. YANG 1993 *AIAA Journal* **31**, 2304–2311. Reliability and nonlinear supersonic flutter of uncertain laminated plates.
12. M. N. BISMARK-NASR 1992 *Applied Mechanics Review* **45**, 461–482. Finite element analysis of aeroelasticity of plates and shell.
13. L. MORINO 1969 *AIAA Journal* **7**, 405–410. A perturbation method for treating nonlinear panel flutter problems.
14. C. C. KUO, L. MORINO and J. DUGUNDJII 1972 *AIAA Journal* **10**, 1479–1484. Perturbation and harmonic balance methods for nonlinear panel flutter.
15. S. W. YUEN and S. L. LAU 1991 *AIAA Journal* **29**, 1472–1479. Effects of inplane load on nonlinear panel flutter by incremental harmonic balance method.
16. C. L. LIAO and Y. W. SUN 1993 *AIAA Journal* **31**, 1897–1905. Flutter analysis of stiffened laminated composite plates and shells in supersonic flow.
17. D. M. LEE and I. LEE 1996 *AIAA Journal* **34**, 637–639. Supersonic flutter analysis of stiffened isotropic and anisotropic panels.
18. D. M. LEE and I. LEE 1997 *Composites & Structures* **63**, 371–378. Vibration behaviors of thermally postbuckled anisotropic plates using first-order shear deformable plate theory.
19. D. M. LEE and I. LEE 1995 *Composites & Structures* **57**, 99–105. Vibration analysis of anisotropic plates with eccentric stiffeners.

APPENDIX

The detailed expression of equation of motion can be written from equation (16) as follows:

$$\begin{bmatrix} [M_m] & [0] & [0] \\ [0] & [M_b] & [0] \\ [0] & [0] & [M_p] \end{bmatrix} \begin{Bmatrix} \{\ddot{u}\} \\ \{\ddot{w}\} \\ \{\ddot{\phi}\} \end{Bmatrix} + g \begin{bmatrix} [0] & [0] & [0] \\ [0] & [A_d] & [0] \\ [0] & [0] & [0] \end{bmatrix} \begin{Bmatrix} \{\dot{u}\} \\ \{\dot{w}\} \\ \{\dot{\phi}\} \end{Bmatrix} + \begin{bmatrix} [K1] & [K2] & [K3] \\ [K2]^{\mathrm{T}} & [K4] & [K5] \\ [K3] & [K5]^{\mathrm{T}} & [K6] \end{bmatrix} \begin{Bmatrix} \{u\} \\ \{w\} \\ \{\phi\} \end{Bmatrix} = \begin{Bmatrix} 0 \\ 0 \\ 0 \end{Bmatrix} \quad \text{(A1)}$$

where

$$[K1] = [K_m], \quad [K2] = [N1_{mb}]_s + \tfrac{1}{2}[N1_{mb}]_t, \qquad [K3] = [K_{mp}],$$
$$[K4] = [K_b] - [K_{\Delta T}] + \beta[A_f] + [N1_b]_s + [N2_b]_s + [N2_b]_{st} + \tfrac{1}{2}[N1_b] + \tfrac{1}{3}[N2_b]_t,$$
$$[K5] = [K_{bp}] + [N1_{bp}]_s + \tfrac{1}{2}[N1_{bp}]_t, \qquad [K6] = [K_p].$$

Applying Guyan reduction to equation (A1), the following reduced equation is obtained.

$$[RM]\{\ddot{w}_t\} + g[A_d]\{\dot{w}_t\} + [\,[RKO] + [RK1] + [RK2]]_t\{w_t\} = \{0\}, \tag{A2}$$

where

$$[RM] = [M_b] + \begin{bmatrix} [K2] \\ [K5]^{\mathrm{T}} \end{bmatrix}^{\mathrm{T}} \begin{bmatrix} [K1] & [K3] \\ [K3]^{\mathrm{T}} & [K6] \end{bmatrix}^{-\mathrm{T}} \begin{bmatrix} [M_m] & [0] \\ [0] & [M_p] \end{bmatrix} \begin{bmatrix} [K1] & [K3] \\ [K3]^{\mathrm{T}} & [K6 \end{bmatrix} \begin{bmatrix} [K2] \\ [K5]^{\mathrm{T}} \end{bmatrix} \tag{A3}$$

and $[RM] \approx [M_b]$ because the second term on the right side of equation (A3) has values of $10^{-3} \simeq 10^{-6}$ order of $[M_b]$ in a plate with $a/c \geqslant 100$. $[RK0]$, $[RK1]$ and $[RK2]$ are given as follows:

$$\begin{aligned}
[RK0] &= [K_b] - [K_{\Delta T}] + \beta[A_f] + [N1_b]_s + [N2_b]_s - [N1_{bm}]_s[\tilde{K}1][N1_{mb}]_s \\
&\quad - [\,[K_{bp}] + [N1_{bp}]_s][\tilde{K}3][N1_{bm}]_s - [N1_{bm}]_s[\tilde{K}3][\,[K_{pb}] + [N1_{pb}]_s] \\
&\quad - [\,[K_{bp}] + [N1_{bp}]_s][\tilde{K}6][\,[K_{pb}] + [N1_{bp}]_s], \\
[RK1] &= \tfrac{1}{2}[N1_b] + [N2_b]_{st} - \tfrac{1}{2}[N1_{bm}]_s[\tilde{K}1][N1_{mb}]_t - \tfrac{1}{2}[N1_{bm}]_t[\tilde{K}1][N1_{mb}]_s \\
&\quad - \tfrac{1}{2}[\,[K_{bp}] + [N1_{bp}]_s][\tilde{K}3]^{\mathrm{T}}[N1_{mb}]_t - \tfrac{1}{2}[N1_{bm}]_s[\tilde{K}3][\,[K_{pb}] + [N1_{pb}]_s] \\
&\quad - \tfrac{1}{2}[N1_{bm}]_s[\tilde{K}3][N1_{pb}]_t - \tfrac{1}{2}[N1_{bp}]_t[\tilde{K}3]^{\mathrm{T}}[N1_{mb}]_s \\
&\quad - \tfrac{1}{2}[\,[K_{bp}] + [N1_{bp}]_s][\tilde{K}6][N1_{pb}]_t - \tfrac{1}{2}[N1_{bp}]_t[\tilde{K}6][\,[K_{pb}] + [N1_{pb}]_s] \\
[RK2] &= \tfrac{1}{3}[N2_b]_t - \tfrac{1}{4}[N1_{bm}]_t[\tilde{K}1][N1_{mb}]_t - \tfrac{1}{4}[N1_{bp}]_t[\tilde{K}3]^{\mathrm{T}}[N1_{mb}]_t \\
&\quad - \tfrac{1}{4}[N1_{bm}]_t[\tilde{K}3][N1_{pb}]_t - \tfrac{1}{4}[N1_{pb}]_t[\tilde{K}6][N1_{pb}]_t
\end{aligned} \tag{A4}$$

where

$$\begin{bmatrix} [\tilde{K}1] & [\tilde{K}3] \\ [\tilde{K}3]^{\mathrm{T}} & [\tilde{K}6] \end{bmatrix} = \begin{bmatrix} [K1] & [K3] \\ [K3]^{\mathrm{T}} & [K6] \end{bmatrix}^{-1}. \tag{A5}$$

The recovery of deleted DOF is carried out using the relationship:

$$\begin{Bmatrix} \{u_t\} \\ \{\phi_t\} \end{Bmatrix} = -\begin{bmatrix} [K1] & [K3] \\ [K3]^{\mathrm{T}} & [K6] \end{bmatrix}^{-1} \begin{bmatrix} [K2] \\ [K5]^{\mathrm{T}} \end{bmatrix} \{w_t\}. \tag{A6}$$